Jet production in deep inelastic *ep* scattering at HERA and determination of α_S

C. Glasman
University of Glasgow, UK

Abstract

Recent measurements of jet cross sections in neutral-current and charged-current deep inelastic *ep* scattering are presented. The results of the QCD analyses on these measurements to determine the strong coupling constant are also reported.

1 Introduction

Jet production in neutral-current (NC) and charged-current (CC) deep inelastic *ep* scattering (DIS) provides a test of perturbative QCD (pQCD) calculations and of the electroweak sector of the Standard Model (SM). Jet cross sections allow the determination of one of the fundamental parameters of QCD, the strong coupling constant α_S, and help to constrain the parton densities in the proton. New particles or interactions may be observed by deviations of the measured jet cross sections with respect to the predictions.

Up to leading order (LO) in α_S, jet production in NC and CC DIS proceeds via the quark-parton model (QPM) ($Vq \to q$, where $V = \gamma$, Z^0 or $W^\pm$), boson-gluon fusion (BGF) ($Vg \to q\bar{q}$) and QCD-Compton (QCDC) ($Vq \to qg$) processes (see figure 1).

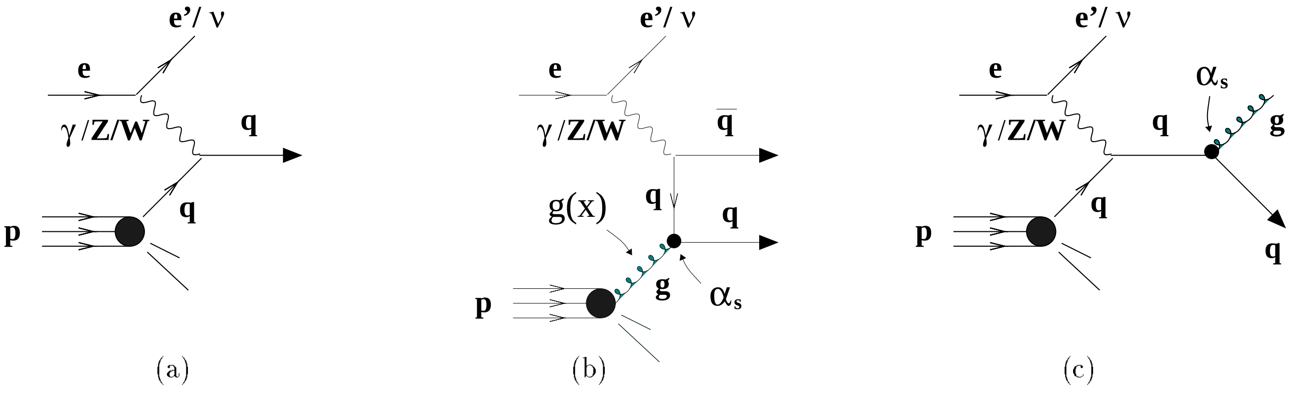

Figure 1: Quark-parton model (a), boson-gluon fusion (b) and QCD Compton (c) diagrams.

The jet production cross section is given in pQCD by the convolution of the parton densities in the proton and the subprocess cross section,

$$d\sigma_{\text{jet}} = \sum_{a=q,\bar{q},g} \int dx\ f_a(x,\mu_F^2)\ d\hat{\sigma}_a(x,\alpha_S(\mu_R),\mu_R^2,\mu_F^2),$$

where x is the fraction of the proton momentum taken by the interacting parton, f_a are the parton distribution functions (PDFs) in the proton, μ_F is the factorisation scale, $\hat{\sigma}_a$ is the subprocess cross section and μ_R is the renormalisation scale.

The proton PDFs are determined from global fits to experimental data (see e.g. [1, 2]) and parametrise the long-distance structure of the target hadron. The subprocess cross section is calculable in pQCD at any order and represents the short-distance structure of the interaction.

The determination of α_S from measurements of cross sections in DIS depends on the proton PDFs. Thus, to perform a QCD analysis, a functional form of the PDFs must be assumed and the determination of α_S should be made from observables with a small dependence on the PDFs, e.g. ratios of observables. For precise measurements of α_S, the experimental and theoretical uncertainties should be small. Small experimental uncertainties are obtained by measuring e.g. ratios of observables and the theoretical uncertainties are reduced by including next-to-leading order (NLO) QCD corrections to the cross section calculations.

2 NLO QCD calculations

Several programs are available to make NLO QCD calculations of jet cross sections in DIS: DISENT [3], MEPJET [4], DISASTER++ [5] and NLOJET [6]. The NLO corrections include virtual corrections with internal particle loops and real corrections with a third parton in the final state. The programs differ in the treatment of the real corrections: DISENT, DISASTER++ and NLOJET use the subtraction method whereas MEPJET uses the phase space slicing method. DISENT and DISASTER++ are found to agree at the 2% level, and NLOJET is in good agreement with them. MEPJET agrees well with the other programs at LO, but presents differences of the order of 5% at NLO. MEPJET is the only program that includes Z^0 and W exchange and only DISASTER++ allows the possibility to turn on the number of active flavours as a function of the scale.

The calculation of jet cross sections at NLO in DIS depends on two scales, μ_R and μ_F. Two possible choices for these scales that have been considered in the analyses presented here are $Q \equiv \sqrt{Q^2}$, where Q^2 is the virtuality of the exchanged boson, and the jet transverse energy, $E_T^{\rm jet}$.

Since the NLO QCD calculations are for jets of partons and the measurements are done at the hadron level, the calculations need to be corrected for hadronisation effects. These effects have been estimated using Monte Carlo models for parton radiation and hadronisation [7, 8].

The uncertainties of the QCD calculations include that due to terms beyond NLO, which is usually estimated by varying the renormalisation scale by factors between 1/2 and 2; it amounts to $5-10\%$ and translates into $\sim 8\%$ in the determination of $\alpha_S(M_Z)$. The uncertainties on the value of $\alpha_S(M_Z)$ and of the proton PDFs amount to $\sim 5\%$. The size and uncertainty of the hadronisation corrections have been taken into account: the hadronisation correction factor amounts to $\sim 5\%$ with an uncertainty of the order of 2%.

3 Inclusive jet cross sections

The use of inclusive jet cross sections in a QCD analysis presents several advantages: inclusive jet cross sections are infrared insensitive and better suited to test resummed calculations and the theoretical uncertainties are smaller than for dijet cross sections.

Inclusive jet cross sections in NC interactions have been measured [9] in the Breit frame using the k_T cluster algorithm [10] in the longitudinally invariant inclusive mode for the kinematic region of $Q^2 > 125$ GeV^2, where Q^2 is the virtuality of the exchanged boson. These cross sections refer to jets of transverse energy measured in the Breit frame, $E_{T,\mathrm{B}}^{\mathrm{jet}}$, above 8 GeV and jet pseudorapidity also in the Breit frame in the range $-2 < \eta_{\mathrm{B}}^{\mathrm{jet}} < 1.8$. The inclusive jet cross sections as a function of Q^2 and $E_{T,\mathrm{B}}^{\mathrm{jet}}$ are shown in figure 2.

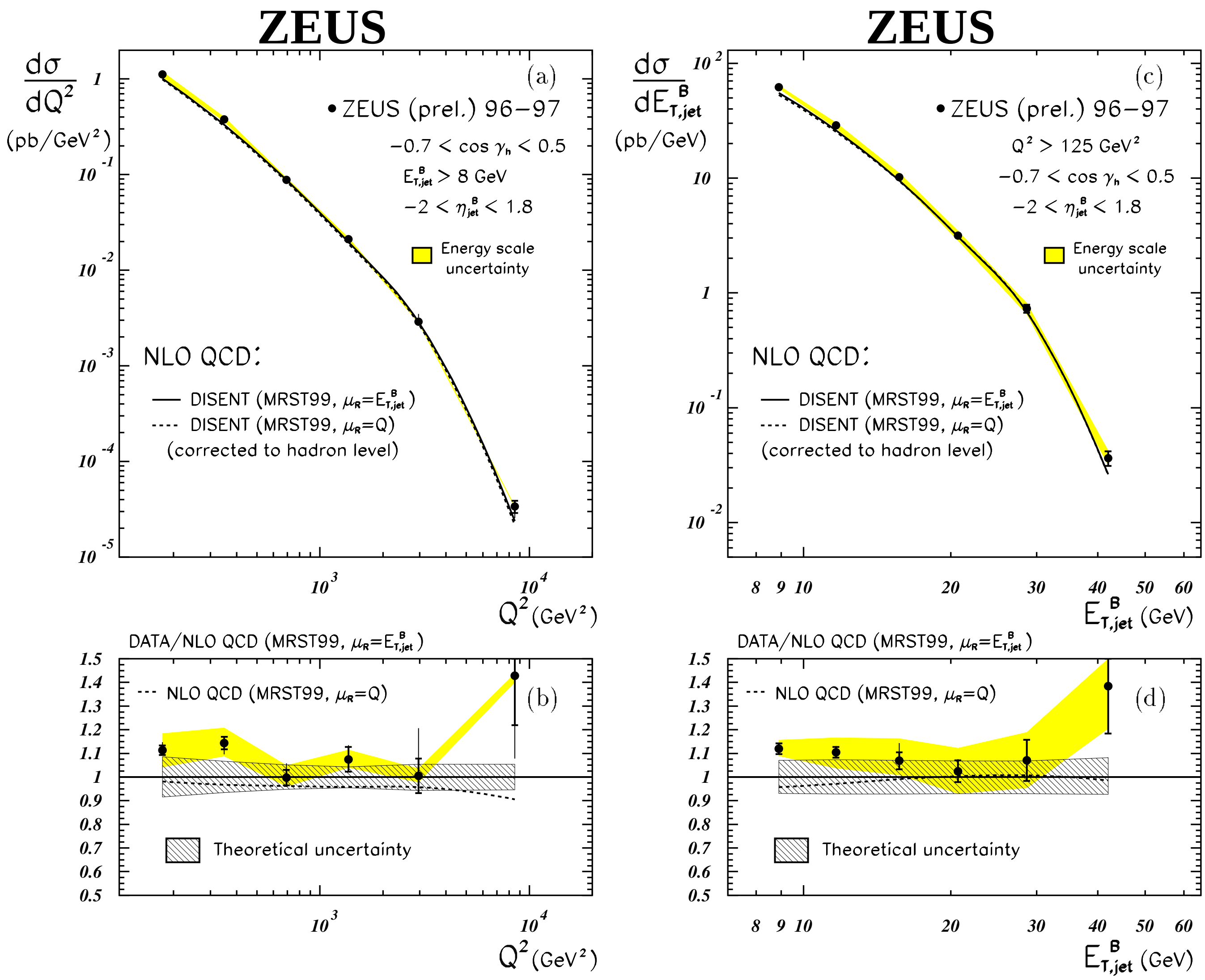

Figure 2: Inclusive jet cross sections in NC DIS as a function of Q^2 (a) and $E_{T,\mathrm{B}}^{\mathrm{jet}}$ (c). Ratio data/theory as a function of Q^2 (b) and $E_{T,\mathrm{B}}^{\mathrm{jet}}$ (d).

The measured cross section has a steep fall-off of five (four) orders of magnitude over the measured range of Q^2 ($E_{T,\mathrm{B}}^{\mathrm{jet}}$). NLO QCD calculations using DISENT, the MRST99 [2] set of proton PDFs and different choices of μ_R have been compared to the data. The calculations describe reasonably well the Q^2 ($E_{T,\mathrm{B}}^{\mathrm{jet}}$) dependence of the cross section for $Q^2 > 500$ GeV^2 ($E_{T,\mathrm{B}}^{\mathrm{jet}} > 15$ GeV).

Inclusive jet cross sections have been measured in the laboratory frame in NC [11] and CC [12] interactions to search for deviations from the SM. The jets have been reconstructed using the k_T cluster algorithm in the kinematic region of $Q^2 > 125$ (200) GeV^2 and at least one jet of $E_T^{\rm jet} > 14$ (8) GeV and $-1 < \eta^{\rm jet} < 2$ for NC (CC) interactions is required.

The inclusive jet cross sections as a function of $E_T^{\rm jet}$ for NC and CC interactions are shown in figure 3. The cross section in NC interactions displays a steep fall-off of four orders of magnitude over the measured range. The behaviour of the $E_T^{\rm jet}$ distribution in CC interactions is very different: it is approximately constant at low $E_T^{\rm jet}$ and falls less rapidly than in NC, and it approaches the NC cross section for $E_T^{\rm jet} \sim 80$ GeV. This behaviour can be interpreted as due to the presence of a massive propagator in CC events, as it has already been observed in measurements of the Q^2 dependence of the inclusive CC DIS cross section [13]. The cross sections for jets give an independent measurement of the different electroweak boson propagators in NC and CC DIS.

The predictions of Monte Carlo models using either the color-dipole model (CDM) [7] or first-order QCD matrix elements plus parton-showers (MEPS) [8] have been compared to the measurements. The calculations describe reasonably well the measured cross sections. No significant deviation from the SM is observed in NC or CC interactions up to the highest $E_T^{\rm jet}$ measured value (~ 100 GeV).

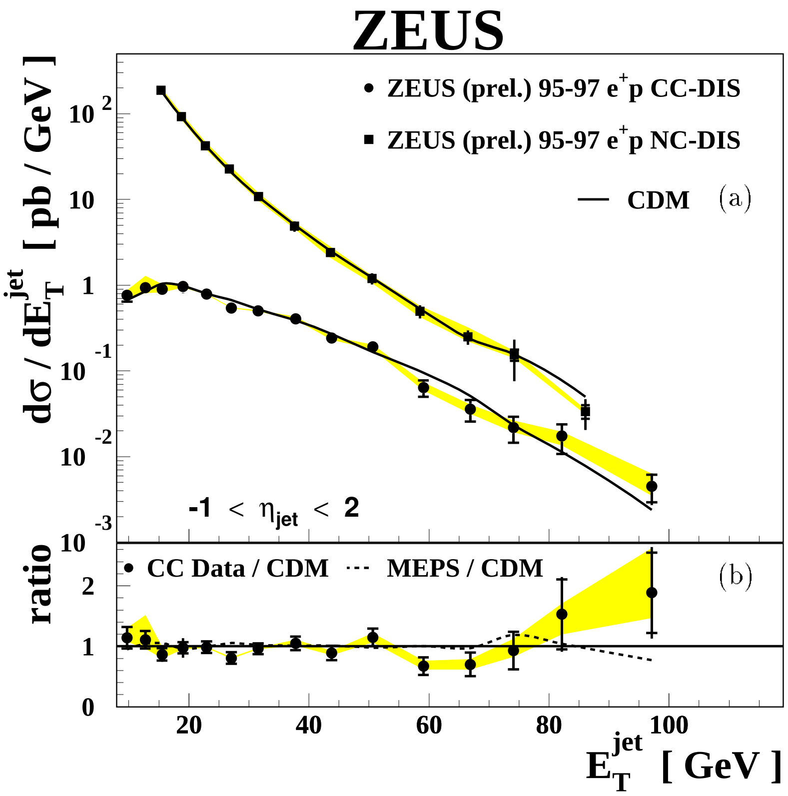

Figure 3: (a) Inclusive jet cross section in NC and CC DIS as a function of $E_T^{\rm jet}$. (b) Ratio data/theory as a function of $E_T^{\rm jet}$ in CC DIS.

4 Dijet cross sections

Differential cross sections for dijet production in NC DIS have been measured [14] in the Breit frame for $470 < Q^2 < 20000$ GeV^2. In this kinematic region, the experimental uncertainties on the reconstruction of both the positron and the hadronic final state are smaller than at lower Q^2. In addition, the theoretical uncertainties due to the modelling of the hadronic final state, to the proton PDFs and to the higher-order contributions are minimised. For these measurements, the k_T cluster algorithm was run in the longitudinally invariant inclusive mode in the Breit frame. Two jets of $E_{T,\mathrm{B}}^{\mathrm{jet,M}} > 8$ GeV, $E_{T,\mathrm{B}}^{\mathrm{jet,m}} > 5$ GeV and $-1 < \eta_{\mathrm{Lab}}^{\mathrm{jet}} < 2$ in each event were required, where $E_{T,\mathrm{B}}^{\mathrm{jet,M}}$ ($E_{T,\mathrm{B}}^{\mathrm{jet,m}}$) is the transverse energy of the jet in the Breit frame with the highest (second highest) transverse energy in the event. The use of asymmetric cuts on $E_{T,\mathrm{B}}^{\mathrm{jet}}$ avoids infrared sensitive regions where the behaviour of the cross section as predicted by the NLO QCD programs is unphysical.

The differential dijet cross sections as functions of $E_{T,\mathrm{B}}^{\mathrm{jet},(1,2)}$, where jet 1 (2) is the jet with highest (lowest) pseudorapidity in the Breit frame, and Q^2 are presented in figure 4. NLO QCD predictions calculated using DISENT are compared to the measurements. The predictions, which assume $\alpha_S(M_Z) = 0.118$, provide a good overall description of both the shape and magnitude of the measured cross sections. The dijet fraction, R_{2+1}, defined as the ratio of the dijet to the inclusive cross section (see figure 5(a)), has been measured as a function of Q^2. The dijet fraction increases with increasing Q^2 due to phase-space effects. For the cross sections as a function of the jet transverse energies and Q^2, there is agreement at the $\approx 10\%$ level between data and theory over four orders of magnitude, demonstrating the validity of the description of the dynamics of dijet production by the NLO QCD hard processes.

Dijet cross sections in CC interactions have been measured [12] in the laboratory frame as a function of the transverse energy of each of the two highest E_T^{jet} jets (figure 6(a)) and as a function of the invariant mass, m_{JJ}, of these two jets (figure 6(b)). The jets have been reconstructed using the k_T cluster algorithm in the kinematic region of $Q^2 > 200$ GeV^2 and at least two jets of $E_T^{\mathrm{jet}} > 8$ GeV and $-1 < \eta^{\mathrm{jet}} < 2$ are required. Values as high as 60 GeV for E_T^{jet} and m_{JJ} are accessible with the luminosity used in this analysis. The shapes of the E_T^{jet} distributions at low E_T^{jet} in inclusive jet (see figure 3) and dijet production are very different: this is interpreted as the inclusive jet cross section being governed by electroweak interactions and the heavy mass of the boson propagator at low E_T^{jet}, whereas the dijet cross section is mainly dictated by QCD. The predictions of the CDM and MEPS models describe reasonably well the shape of the measured dijet cross sections, but they underestimate the normalisation by $\sim 50\%$; this is understood since these models only include up to $\mathcal{O}(\alpha_S)$ diagrams.

5 Jet substructure

The investigation of the internal structure of jets gives insight into the transition between a parton produced in a hard process and the experimentally observed spray of hadrons. At sufficiently high E_T^{jet}, where fragmentation effects become negligible, the jet structure is expected to be calculable in pQCD. The lowest non-trivial order contribution to the measurements of jet substructure is given by $\mathcal{O}(\alpha\alpha_S)$ calculations. Thus, measurements of jet substructure provide a stringent test of pQCD and allow a determination of α_S by comparing NLO calculations to the measurements. At present, this is only possible for jets defined in the laboratory frame since only in this frame can three partons be inside one jet (see figure 7).

The jet substructure was studied by means of the integrated jet shape in inclusive jet production in NC interactions [15] using the k_T cluster algorithm in the laboratory frame. The integrated jet shape is defined as the average fraction of the jet's transverse energy that lies inside a cone in the $\eta - \varphi$ plane of radius r concentric with the jet axis,

$$\langle \psi(r) \rangle = \frac{1}{N_{\mathrm{jets}}} \sum_{\mathrm{jets}} \frac{E_T(r)}{E_T^{\mathrm{jet}}},$$

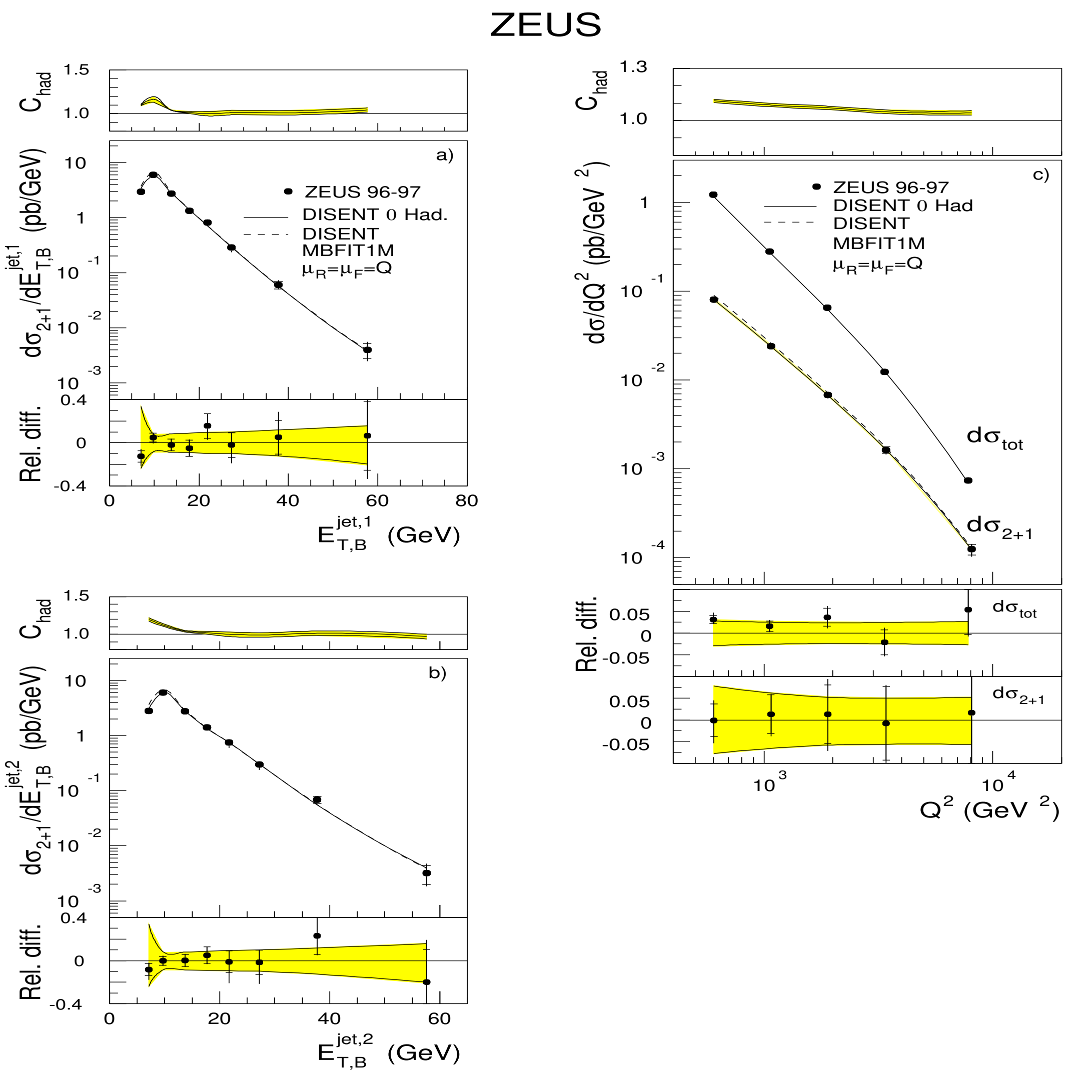

Figure 4: Dijet cross sections in NC DIS as functions of (a) $E_{T,\mathrm{B}}^{\mathrm{jet},1}$, (b) $E_{T,\mathrm{B}}^{\mathrm{jet},2}$ and (c) Q^2. In (c), the inclusive differential cross section ($d\sigma_{\mathrm{tot}}$) is also shown as a function of Q^2.

where $E_T(r)$ is the transverse energy associated with the jet within the given cone of radius r and N_{jets} is the total number of jets in the sample. Only the particles assigned to the jet are considered. The integrated jet shape as a function of the radius r in different regions of E_T^{jet} is shown in figure 8.

In pQCD, $\langle 1-\psi(r)\rangle$ is calculated as the fraction of the jet's transverse energy, due to parton emission, that lies outside of the cone of radius r,

$$\langle 1-\psi(r)\rangle = \frac{\int dE_T \; E_T \; [d\sigma(ep \to 2 \text{ partons})/dE_T]}{E_T^{\mathrm{jet}} \; \sigma_{\mathrm{jet}}(E_T^{\mathrm{jet}})},$$

where $\sigma_{\mathrm{jet}}(E_T^{\mathrm{jet}})$ is the cross section for inclusive jet production. NLO QCD predictions for the integrated jet shape are derived from the above formula by computing the numerator to $\mathcal{O}(\alpha\alpha_S^2)$ and the denominator to $\mathcal{O}(\alpha\alpha_S)$. Calculations using DISENT have been compared to the data. They give a very good description of the measurements for $r \geq 0.2$ (see figure 8).

The jet substructure was also studied by means of the mean subjet multiplicity in NC [15] and CC [12] interactions. Subjets are jet-like objects within a jet which are resolved by reapplying

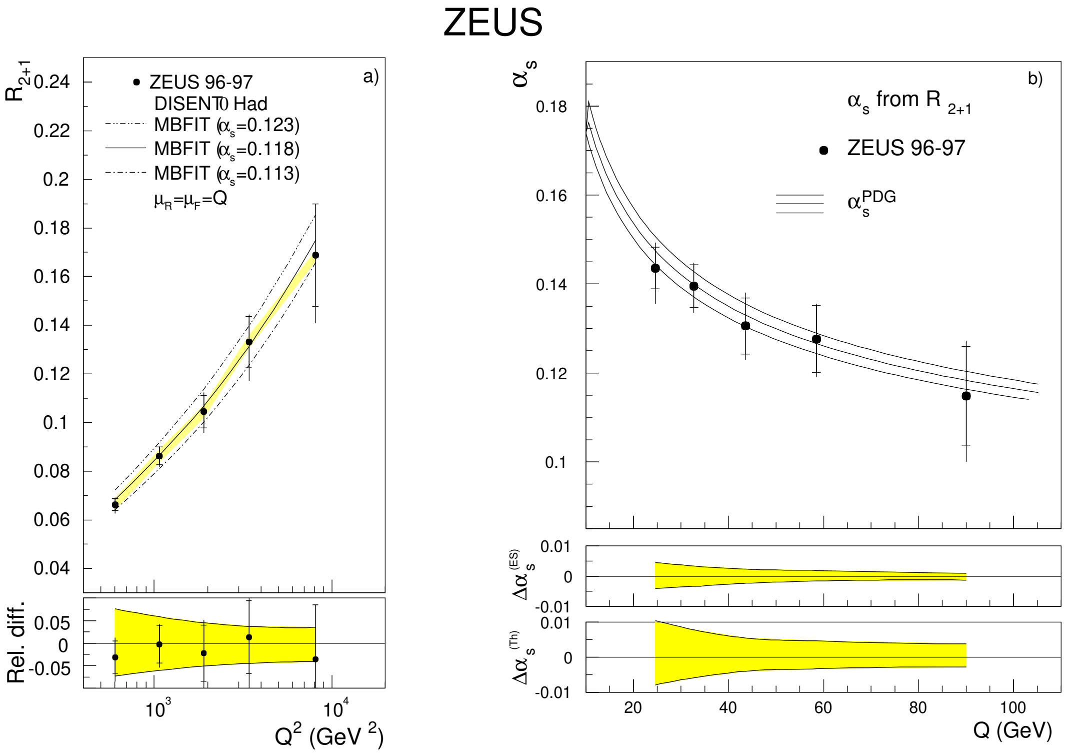

Figure 5: (a) The dijet fraction, R_{2+1}, in NC DIS as a function of Q^2. (b) The α_S values determined from the QCD fit of the measured dijet fraction R_{2+1} as a function of Q.

the k_T cluster algorithm until for every pair of particles the quantity

$$d_{ij} = \min(E_{T,i}, E_{T,j})^2[(\eta_i - \eta_j)^2 + (\varphi_i - \varphi_j)^2]$$

is above $y_{\rm cut} \cdot (E_T^{\rm jet})^2$, where $y_{\rm cut}$ is the resolution parameter.

The mean subjet multiplicity as a function of the resolution parameter $y_{\rm cut}$ is presented in figure 9 for NC interactions. In pQCD, $\langle n_{\rm subjet} - 1\rangle$ is calculated as the ratio of the cross section for $n_{\rm subjet} - 1$ subjets over that of inclusive jet production,

$$\langle n_{\rm subjet} - 1\rangle = \frac{\sigma_{\rm n_{subjet}-1}(E_T^{\rm jet})}{\sigma_{\rm jet}(E_T^{\rm jet})}.$$

NLO QCD predictions for the mean subjet multiplicity are derived from the above formula by adding 1 and computing the numerator (denominator) to $\mathcal{O}(\alpha\alpha_S^2)$ ($\mathcal{O}(\alpha\alpha_S)$). NLO calculations computed using DISENT and different parametrisations of the proton PDFs, which were determined assuming different values of α_S, have been compared to the data. The NLO QCD calculation using the CTEQ4M proton PDFs and $\alpha_S(M_Z) = 0.116$ gives a good description of the measurements.

The measured mean subjet multiplicity as a function of $y_{\rm cut}$ for different regions in $\eta^{\rm jet}$ and $E_T^{\rm jet}$ is shown in figures 10 and 11, respectively, for CC interactions. The predicted mean subjet multiplicities at the hadron level using the CDM and MEPS models have been compared to the measurements. The measured mean subjet multiplicities are well described by the predictions.

The $E_T^{\rm jet}$ dependence of the integrated jet shape at a fixed value of $r = 0.5$ (figure 12(a)) and that of the mean subjet multiplicity at a fixed value of $y_{\rm cut} = 10^{-2}$ (figure 12(b)) in NC interactions have also been studied [15]. The jet shape increases and the subjet multiplicity decreases

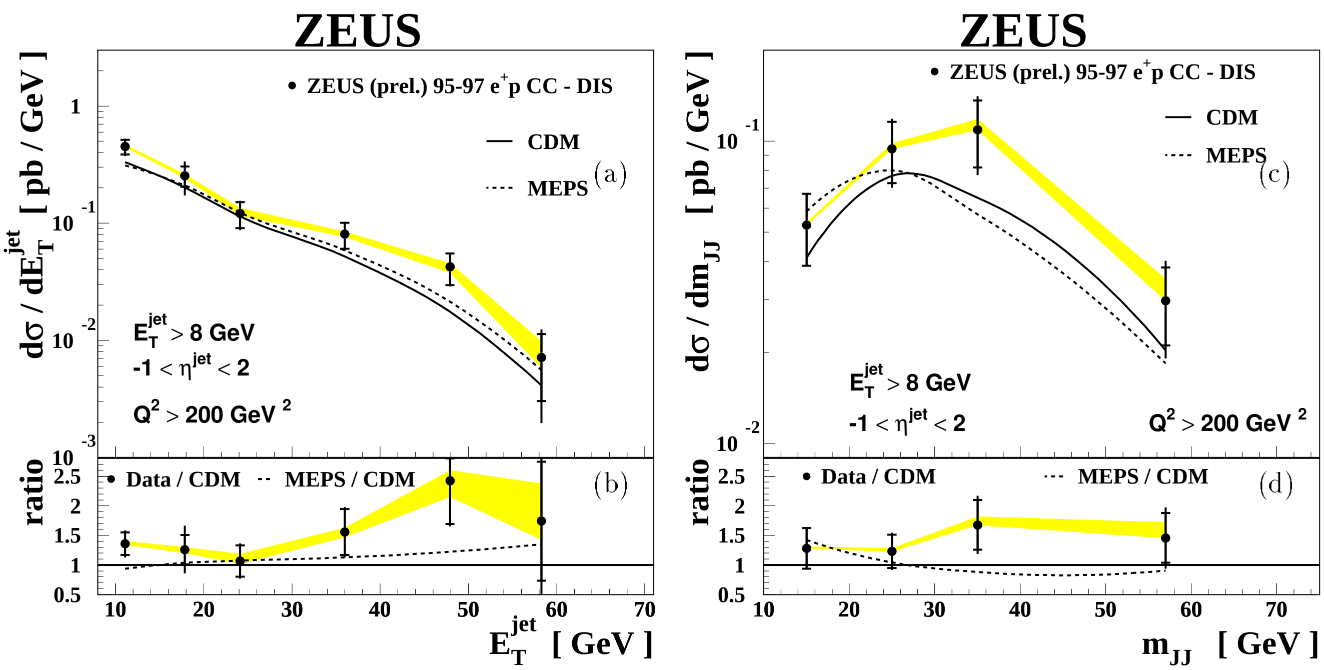

Figure 6: Dijet cross sections in CC DIS as a function of $E_T^{\rm jet}$ (a) and m_{JJ} (c). Ratio data/theory as a function of $E_T^{\rm jet}$ (b) and m_{JJ} (d).

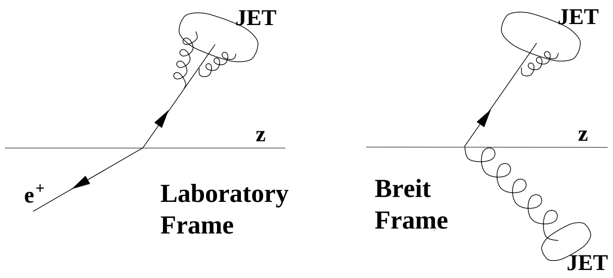

Figure 7: Diagrams in $\mathcal{O}(\alpha\alpha_S^2)$ calculations.

as $E_T^{\rm jet}$ increases: the jets become narrower as $E_T^{\rm jet}$ increases. NLO QCD calculations using DISENT and different parametrisations of the PDFs have been compared to the data. They give a good description of the measurements and display the sensitivity of these observables to α_S.

Figure 13(a) shows the measured $\langle n_{\rm subjet}\rangle$ at $y_{\rm cut} = 10^{-2}$ as a function of $\eta^{\rm jet}$ in CC interactions. It exhibits no significant dependence on $\eta^{\rm jet}$, as in the case of the jet shape [16]. The measured $\langle n_{\rm subjet}\rangle$ at $y_{\rm cut} = 10^{-2}$ as a function of $E_T^{\rm jet}$ is presented in figure 13(b). It decreases as $E_T^{\rm jet}$ increases and thus the jets become narrower as $E_T^{\rm jet}$ increases. In both figures, the predictions from the CDM model are in good agreement with the data whereas the predictions from the MEPS model are slightly above the data. In figure 13(b), the measurements from figure 12(b) are also shown. The measured $\langle n_{\rm subjet}\rangle$ at $y_{\rm cut} = 10^{-2}$ in CC and NC are very similar. This similarity can be attributed to a large content of final-state quark jets in these two processes and shows that the pattern of QCD radiation close to a primary quark is to a large extent independent of the hard scattering process.

ZEUS

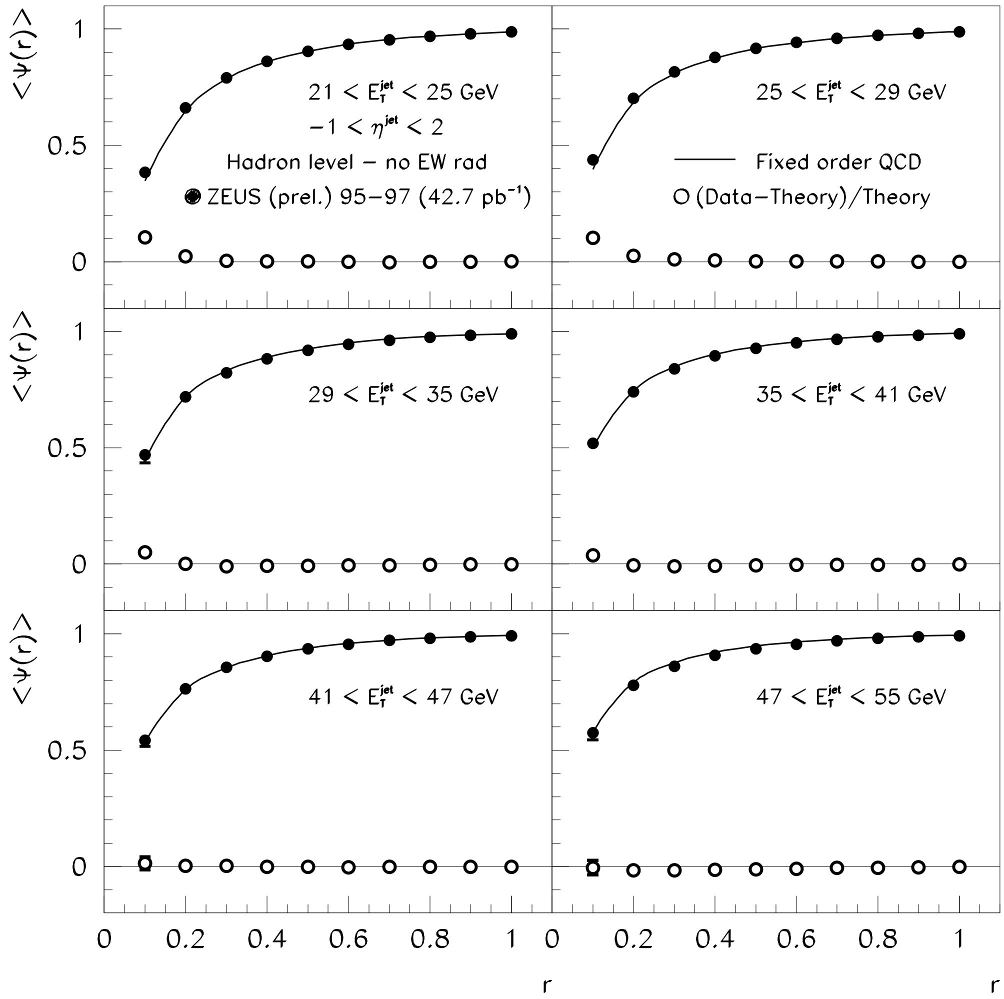

Figure 8: Integrated jet shape as a function of r in different regions of $E_T^{\rm jet}$ in NC DIS.

6 QCD analyses

6.1 Determination of α_S

In recent publications [9, 14, 15], a new method to determine α_S has been presented. The method consists of performing NLO calculations of an observable using the five CTEQ4 sets of the "A-series" [1]; the value of $\alpha_S(M_Z)$ in each calculation is that of the corresponding set of PDFs. The calculations for each $\alpha_S(M_Z)$ are used to parametrise the α_S dependence of the observables, and then, from the measurements, a value of $\alpha_S(M_Z)$ is directly extrapolated. The measurements of the inclusive jet cross section [9] and the dijet fraction [14] as a function of Q^2 and the integrated jet shape [15] and mean subjet multiplicity [15] as a function of $E_T^{\rm jet}$ have been used to determine a value of $\alpha_S(M_Z)$.

From each measurement in a given Q^2 or $E_T^{\rm jet}$ region, a value of $\alpha_S(M_Z)$ was determined. The results are shown in figure 14 separately for the inclusive jet cross section, the mean subjet multiplicity and the integrated jet shape.

A combined value of $\alpha_S(M_Z)$ from each observable has been obtained by performing a χ^2 fit to the data in the following kinematic ranges: $Q^2 > 500$ GeV^2 for the inclusive jet cross section, $Q^2 > 470$ GeV^2 for the dijet fraction, $E_T^{\rm jet} > 21$ GeV for the integrated jet shape and $E_T^{\rm jet} > 25$ GeV for the mean subjet multiplicity. These are the kinematic regions where the hadronisation correction factors to the NLO calculations are small for each observable. The

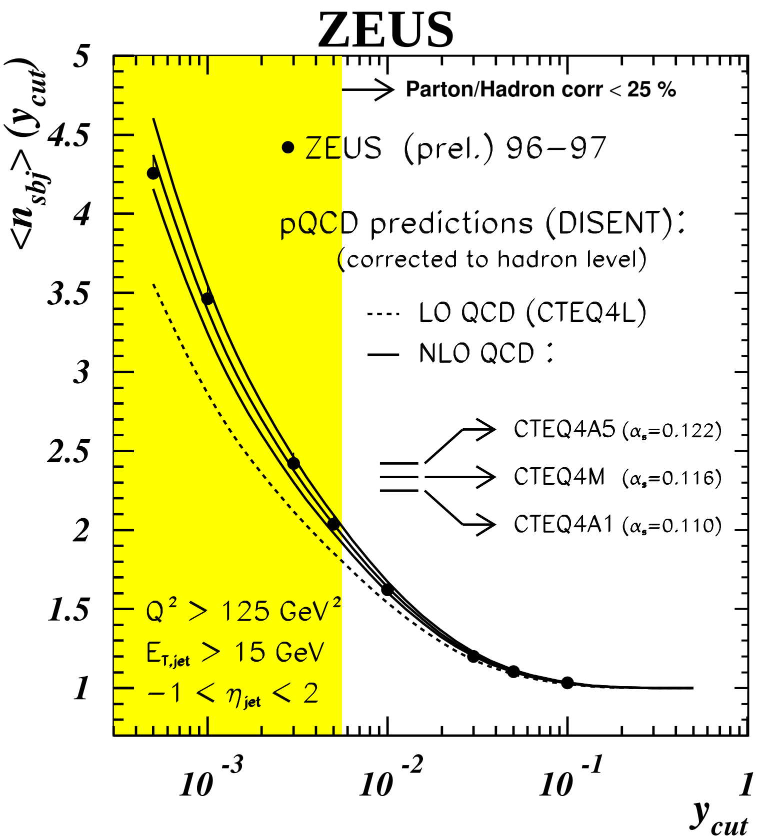

Figure 9: Mean subjet multiplicity as a function of $y_{\rm cut}$ in NC DIS.

combined values of $\alpha_S(M_Z)$ determined from each observable are:

inclusive jet cross section:	$\alpha_S(M_Z) = 0.1190 \pm 0.0017\ (\rm stat)\ ^{+0.0049}_{-0.0023}\ (\rm exp)\ ^{+0.0026}_{-0.0026}\ (\rm th)$;
dijet fraction:	$\alpha_S(M_Z) = 0.1166 \pm 0.0019\ (\rm stat)\ ^{+0.0024}_{-0.0033}\ (\rm exp)\ ^{+0.0057}_{-0.0044}\ (\rm th)$;
integrated jet shape:	$\alpha_S(M_Z) = 0.1179 \pm 0.0014\ (\rm stat)\ ^{+0.0054}_{-0.0065}\ (\rm exp)\ ^{+0.0094}_{-0.0073}\ (\rm th)$;
mean subjet multiplicity:	$\alpha_S(M_Z) = 0.1185 \pm 0.0016\ (\rm stat)\ ^{+0.0067}_{-0.0048}\ (\rm exp)\ ^{+0.0089}_{-0.0071}\ (\rm th)$.

The values of $\alpha_S(M_Z)$ obtained from the different observables are compatible with each other and with the world average [17, 18] (see figure 15).

6.2 Energy scale dependence of α_S

The QCD fit of the dijet fraction has been repeated in five Q^2 bins to test the scale dependence of the renormalised strong coupling constant. The method of the fit is the same as outlined above, but the α_S dependence of the dijet fraction was parametrised in terms of $\alpha_S(\langle Q\rangle)$, where $\langle Q\rangle$ is the mean value of Q in each bin. The measured $\alpha_S(\langle Q\rangle)$ values are shown in figure 5(b). The measurements are compared with the renormalisation group predictions obtained from the PDG $\alpha_S(M_Z)$ value and its associated uncertainty. The values are in good agreement with the predicted running of the strong coupling constant over a large range in Q.

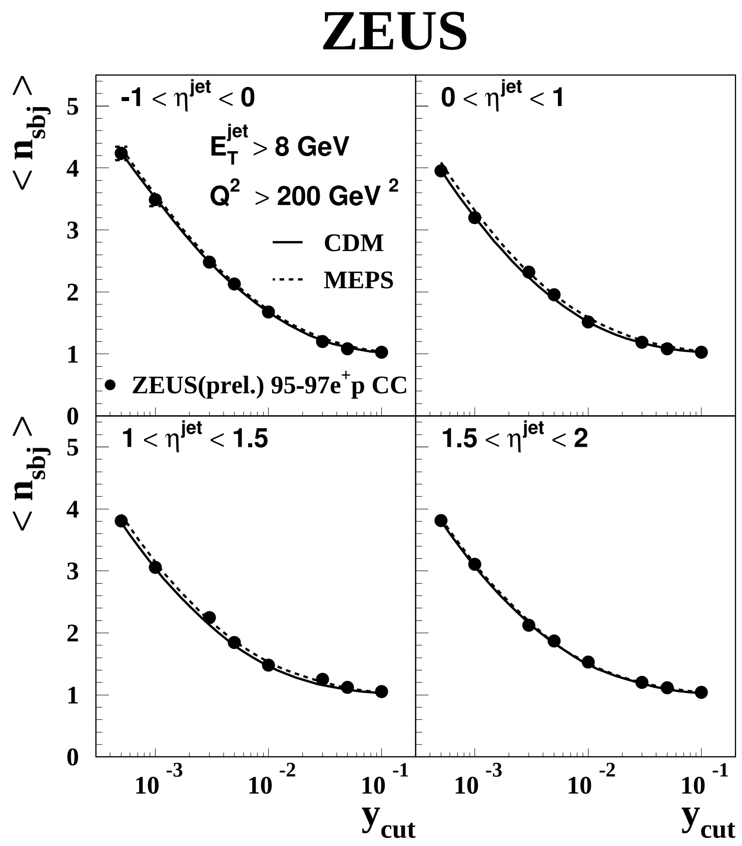

Figure 10: Mean subjet multiplicity as a function of $y_{\rm cut}$ in different $\eta^{\rm jet}$ regions in CC DIS.

7 Summary and conclusions

Recent measurements of jet cross sections in neutral-current and charged-current deep inelastic ep scattering have been presented. From QCD analyses of these measurements, determinations of the strong coupling constant α_S have been obtained. The results are consistent with the world average value of $\alpha_S(M_Z)$. The measurements have been performed in regions of phase space where the experimental uncertainties are small and thus the determinations are precise.

However, the next-to-leading order (NLO) calculations used in the QCD analyses have relatively large uncertainties. For more accurate measurements of the parameters of QCD, improved calculations are needed. For instance, higher-order corrections are required to reduce the largest theoretical uncertainty, namely that of the terms beyond NLO.

Acknowledgments. This report is partially based on a talk given at the *International Europhysics Conference on High Energy Physics*, Budapest, Hungary, July 2001. I would like to thank J. Terrón for a critical reading of the manuscript.

References

[1] H.L. Lai *et al*, *Phys. Rev.* **D** 55 (1997) 1280.

[2] A.D. Martin *et al*, *Eur. Phys. Jour.* **C** 14 (2000) 133.

[3] S. Catani and M. H. Seymour, *Nucl. Phys.* **B** 485 (1997) 291; Erratum **B** 510 (1997) 503.

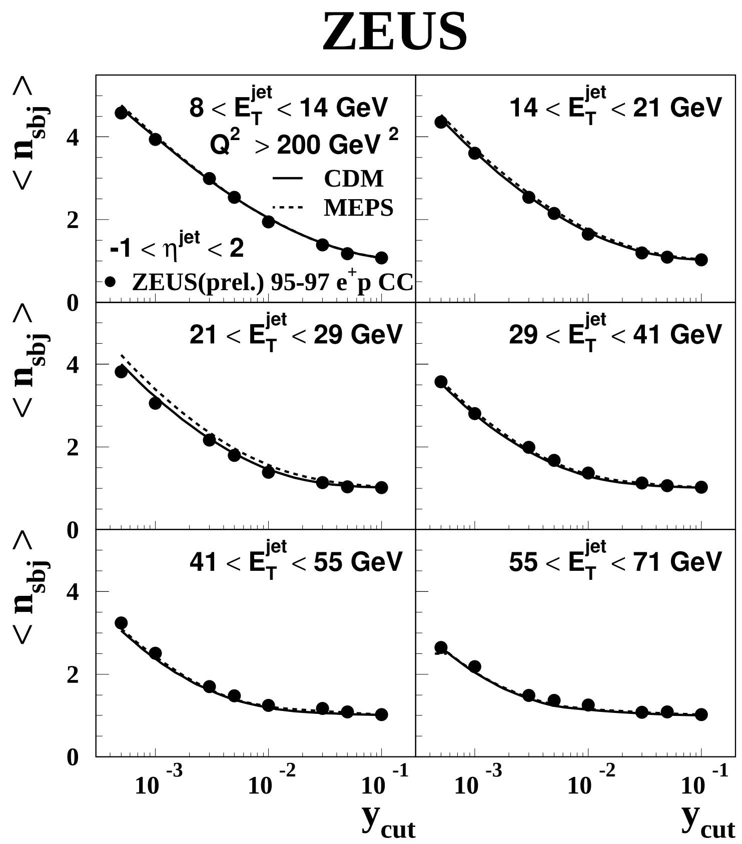

Figure 11: Mean subjet multiplicity as a function of $y_{\rm cut}$ in different $E_T^{\rm jet}$ regions in CC DIS.

[4] E. Mirkes and D. Zeppenfeld, *Phys. Lett.* **B** 380 (1996) 205; E. Mirkes, TTP-97-39 (hep-ph/9711224).

[5] D. Graudenz, hep-ph/9710244.

[6] Z. Nagy and Z. Trocsanyi, hep-ph/0104315.

[7] Y. Azimov *et al*, *Phys. Lett.* **B** 165 (1985) 147; G. Gustafson, *Phys. Lett.* **B** 175 (1986) 453; G. Gustafson and U. Petersson, *Nucl. Phys.* **B** 306 (1988) 746; B. Andersson, G. Gustafson and L. Lönnblad, *Z. Phys.* **C** 43 (1989) 625.

[8] G. Ingelman, A. Edin and J. Rathsman, *Comp. Phys. Comm.* 101 (1997) 108.

[9] ZEUS Collaboration, "Inclusive jet cross sections in neutral current deep inelastic scattering in the Breit frame and determination of α_S at HERA ", paper 637, submitted to the International Europhysics Conference on High Energy Physics 2001, Budapest (2001).

[10] S. Catani *et al*, *Nucl. Phys.* **B** 406 (1993) 187; S.D. Ellis and D.E. Soper, *Phys. Rev.* **D** 48 (1993) 3160.

[11] ZEUS Collaboration, "Inclusive jet cross sections in deep inelastic *ep* scattering at high Q^2", paper 536, submitted to the International Europhysics Conference on High Energy Physics 1999, Tampere (1999).

[12] ZEUS Collaboration, "Measurements of jet cross sections and jet substructure in charged current deep inelastic scattering at HERA", paper 646, submitted to the International Europhysics Conference on High Energy Physics 2001, Budapest (2001).

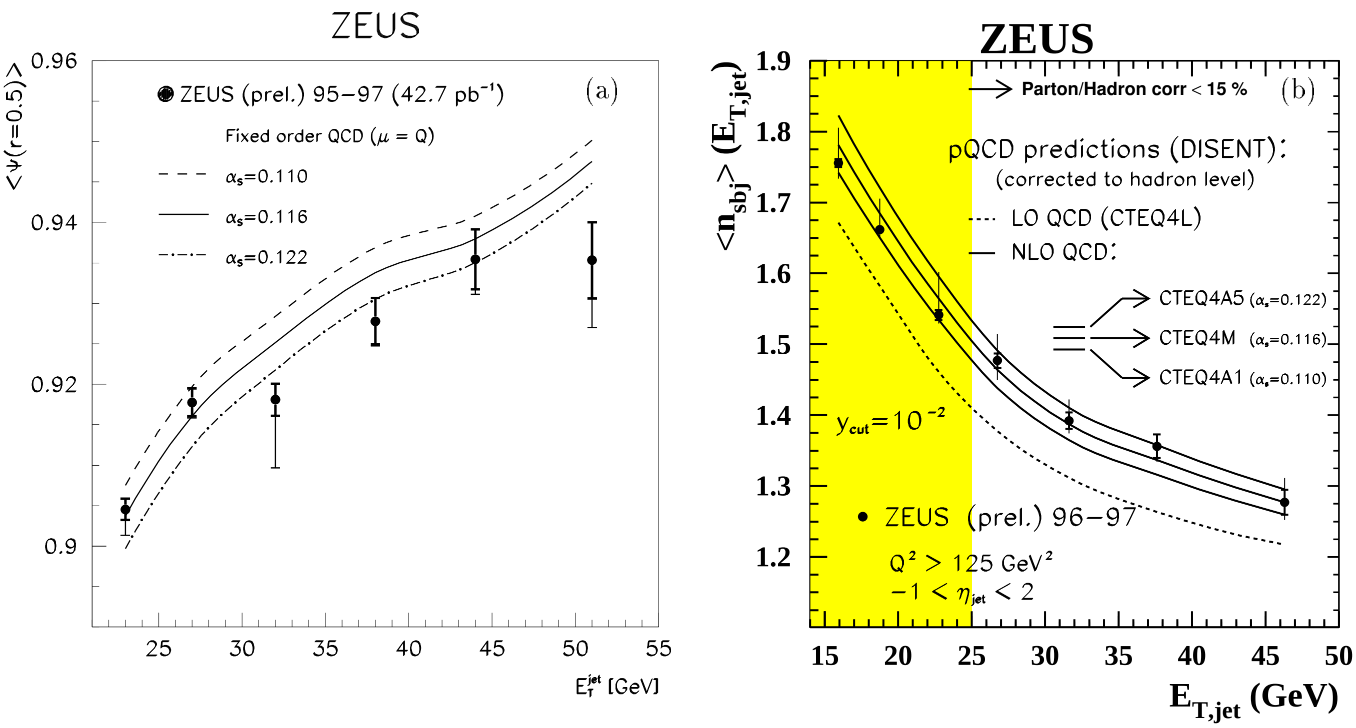

Figure 12: Integrated jet shape at a fixed value of $r = 0.5$ (a) and mean subjet multiplicity at a fixed value of $y_{\rm cut} = 10^{-2}$ (b) as a function of $E_T^{\rm jet}$ in NC DIS.

[13] ZEUS Collaboration, J. Breitweg *et al*, *Eur. Phys. Jour.* **C** 12 (2000) 411.

[14] ZEUS Collaboration, J. Breitweg *et al*, *Phys. Lett.* **B** 507 (2001) 70.

[15] ZEUS Collaboration, "Measurements of jet substructure in neutral current deep inelastic scattering and determination of α_S at HERA", paper 641, submitted to the International Europhysics Conference on High Energy Physics 2001, Budapest (2001).

[16] ZEUS Collaboration, J. Breitweg *et al*, *Eur. Phys. Jour.* **C** 8 (1999) 367.

[17] Particle Data Group, D.E. Groom *et al*, *Eur. Phys. Jour.* **C** 15 (2000) 1.

[18] S. Bethke, *J. Phys.* **G** 26 (2000) R27.

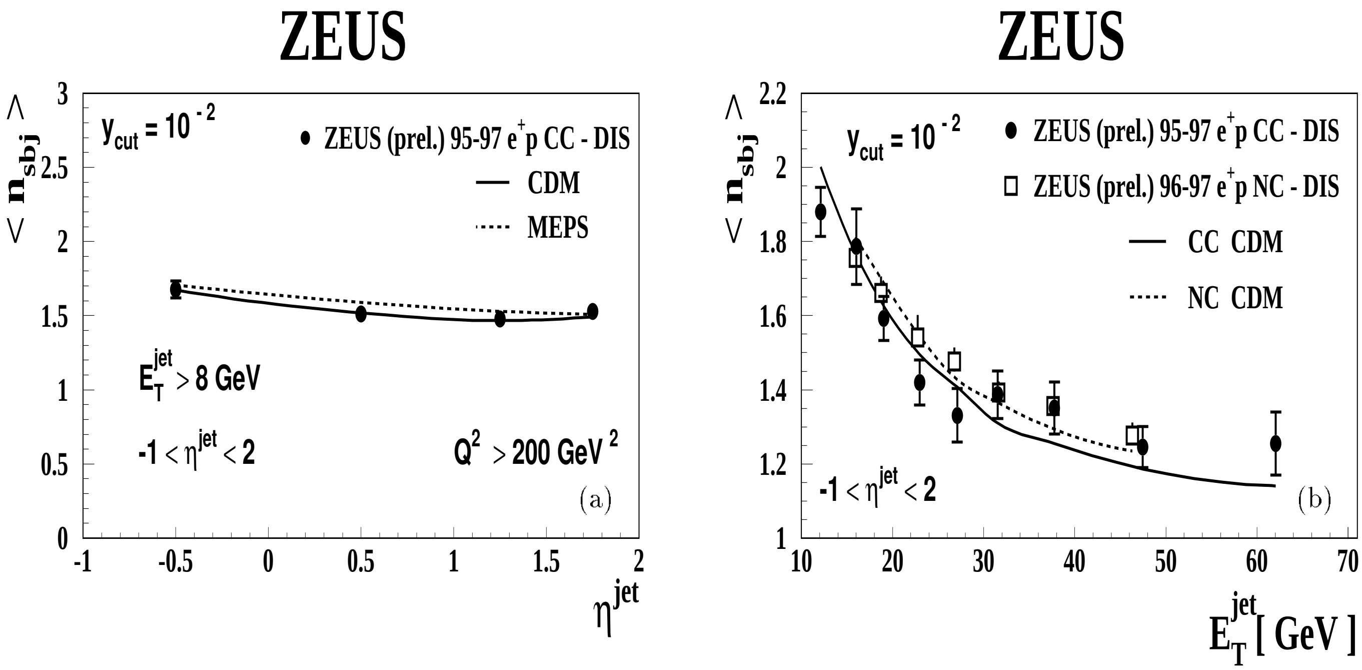

Figure 13: Mean subjet multiplicity at a fixed value of $y_{\text{cut}} = 10^{-2}$ as a function of (a) η^{jet} and (b) E_T^{jet} in CC DIS.

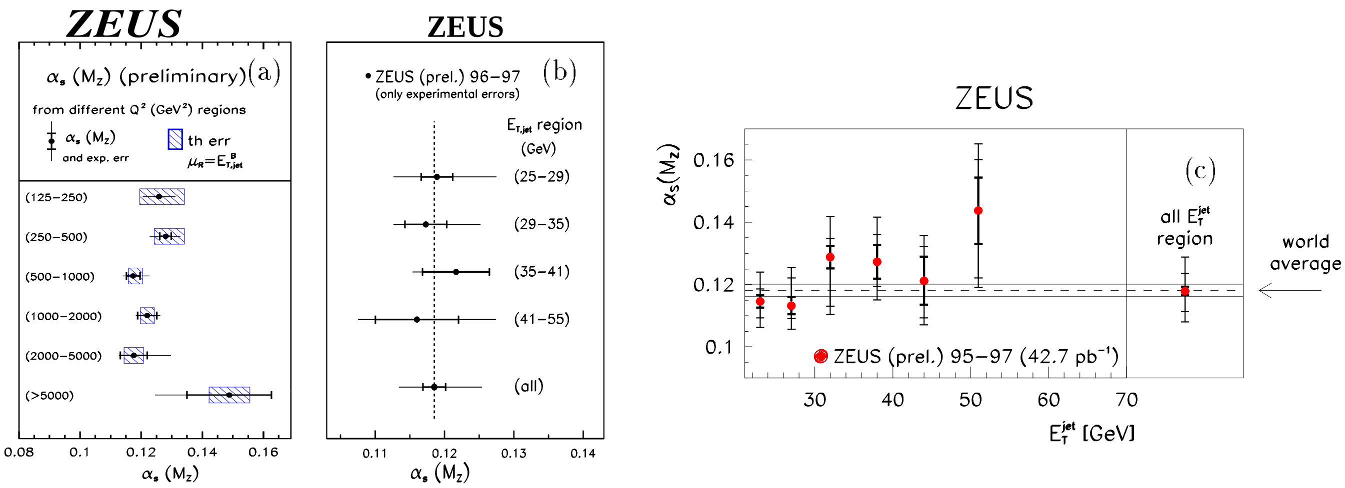

Figure 14: Extracted values of $\alpha_S(M_Z)$ from the inclusive jet cross section (a), the mean subjet multiplicity (b) and the integrated jet shape (c) in NC DIS.

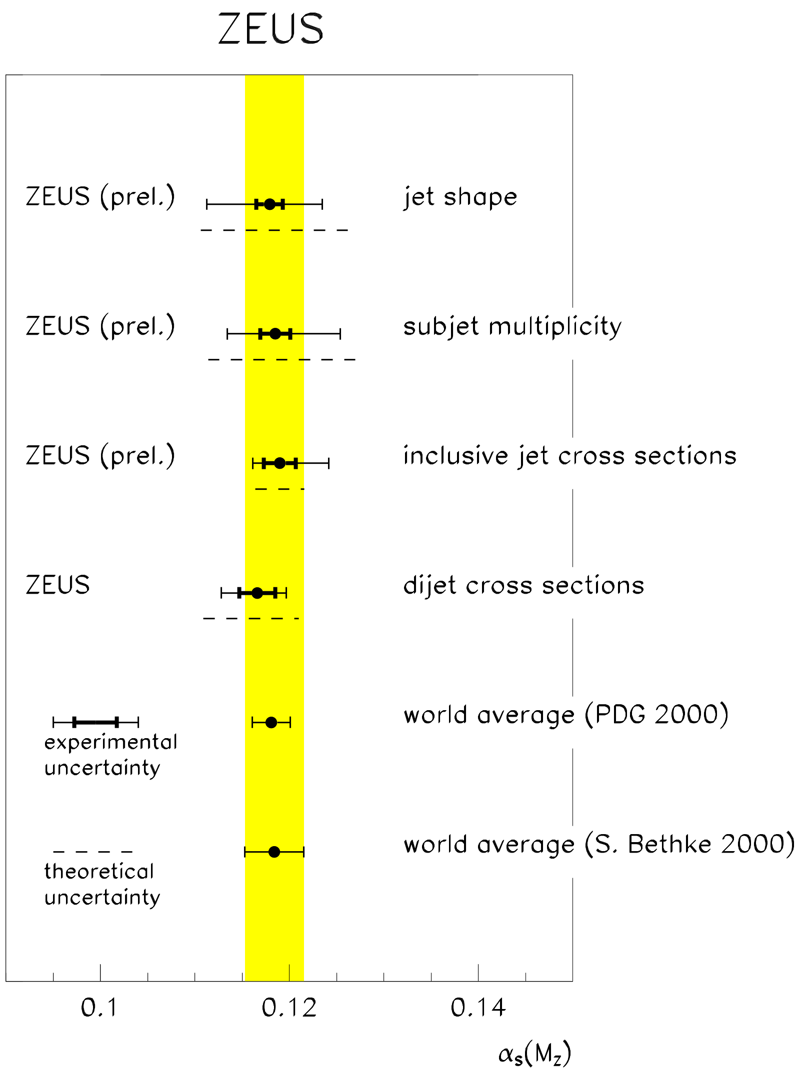

Figure 15: A compilation of recent determinations of $\alpha_S(M_Z)$ using jet production in NC DIS.